Laser power requirement for cutting thick-section steel and effects of processing parameters on mild steel cut quality

C Wandera[1]*, V Kujanpää[1,2], and **A Salminen[1,3]**
[1]Department of Mechanical Engineering, Lappeenranta University of Technology, Lappeenranta, Finland
[2]VTT The Technical Research Centre of Finland, Lappeenranta, Finland
[3]Machine Technology Centre Turku Limited, Turku, Finland

The manuscript was received on 7 January 2010 and was accepted after revision for publication on 7 May 2010.

DOI: 10.1177/09544054JEM1971

Abstract: The high-power fibre laser presents a possibility for the application of solid-state lasers in thick-section metal cutting, a field which has been dominated by high-power CO_2 lasers. The current paper presents the lumped-parameter formulation of the laser power requirement as a function of cutting speed for oxygen-assisted laser cutting of mild steel and nitrogen-assisted laser cutting of stainless steel. The calculated laser power requirement is compared with the incident laser power used in the cutting of 15 mm mild steel with oxygen assist gas and 10 mm stainless steel with nitrogen assist gas using a multi-mode 5 kW fibre laser and a 4 kW CO_2 laser. The incident laser power required for cutting at a given cutting speed is found to be lower for fibre laser cutting than for the CO_2 laser cutting, indicating a higher absorption of the fibre laser beam. The effects of process parameters on the cut kerf quality in mild steel laser cutting with oxygen assist gas using the high-power fibre laser are presented. The critical process parameters affecting the quality of the cutting process and the resulting cut kerf are the cutting speed, oxygen pressure, and nozzle diameter.

Keywords: laser cutting, thick section, mild steel, stainless steel, fibre laser, CO_2 laser

1 INTRODUCTION

Laser cutting of a steel workpiece is achieved by application of a high-intensity focused laser beam to melt the kerf volume and an assist gas jet to blow the melt out of the cut kerf. The most productive method for laser cutting of mild steel in industry is to use an oxygen assist gas jet to ignite and carry on an exothermic reaction between iron and oxygen. The exothermic reaction acts as an additional power source for the cutting process, resulting in higher cutting speeds. The downside of this process is the oxidized cut edges. The presence of the oxide layer on the cut edge may influence the final quality during further processing operations such as welding or painting. The oxide layer may need to be removed in a cleaning operation prior to further processing of the part. Stainless steel laser cutting is often performed using nitrogen assist gas to give clean cut surfaces which do not require any cleaning operation of the oxide layer. Inert gas-assisted laser cutting of thin- and medium-section stainless steel using the high-power fibre laser has been tested by the authors [**1**] and other researchers [**2**], and higher cutting speeds have been reported compared with CO_2 laser cutting. It is now anticipated that the use of the high-power fibre laser for the cutting of thick-section steel will offer competitive performance and advantages to challenge the CO_2 laser which is currently dominating this application area of laser materials processing in industry. Larger cut depths and higher cutting speeds are expected when the fibre laser is used to cut metal workpieces than when a CO_2 laser is used, because the shorter wavelength of the fibre laser (1.06 μm) is more highly absorbed by metal workpieces than the longer wavelength of the CO_2 laser (10.6 μm). The absorptivity also depends on the temperature and

**Corresponding author: Department of Mechanical Engineering, Lappeenranta University of Technology, Tuotantokatu 2, 53850 Lappeenranta, Finland.*
email: cathywandera@yahoo.com

phase of the material such that the absorptivity increases with increase in workpiece temperature [**3**]. The cutting speeds of the high-power fibre laser have been reported to be more than double those of the CO_2 laser for thin-section to medium-section cutting of stainless steel, but relatively similar cutting speeds have been reported in the cutting of thickness greater than 6 mm. However, thick-section metal cutting using the high-power fibre laser has been reported to produce poorer cut quality with more complex striation patterns than typical in CO_2 laser cutting. Mahrle *et al.* [**4**] reported that the main reason for the poor cut edge quality obtained with the fibre laser compared with the CO_2 laser is the different wavelength, which leads to different absorption mechanisms. They argued that there is a distinct angle of incidence, corresponding to 85.9°, above which the absorptivity of the CO_2 laser radiation is better than the absorptivity of the fibre laser radiation; also that fibre laser cutting works in a regime where the absorptivity is not optimal in relation to the cut front angle, while optimum cut front inclination is achieved with CO_2 laser radiation for optimal absorptivity in a wide range of material thickness.

The influence of laser cutting parameters on the cut quality in thin-section steel has been widely investigated by various authors. Golnabi and Bahar [**5**] investigated the optimum conditions for minimum kerf width during oxygen-assisted laser cutting of thin-section (1 mm, 1.5 mm, and 2 mm) stainless steel and mild steel using an Nd:YAG laser and observed that cutting of mild steel required a lower oxygen gas pressure than stainless steel cutting and the kerf width in mild steel was larger than that in stainless steel. They reported a minimum kerf width of 0.3 mm in 1 mm thick mild steel with 1 bar oxygen pressure (67 W laser power and 9.5 mm/s cutting rate), while a minimum kerf width of 0.2 mm was obtained in 1 mm thick stainless steel with 4 bar oxygen pressure (67 W laser power, 7.1 mm/s cutting rate). Yilbas [**6**] investigated the influence of process parameters during CO_2 laser cutting of thin-section (0.75, 1.0, and 1.5 mm) mild steel sheets with oxygen assist gas and reported that the heat spread from the cutting zone decreased at high cutting speeds, resulting in increased temperature gradients in the kerf and minimal tendency for self-sustaining oxidation reaction. He also reported that a substantial amount of surface plasma occurred periodically during cutting of thicker workpieces with high oxygen pressure, causing increased erosion of the cut edge and development of striations on the cut edge. On the contrary, Powell *et al.* [**7**] disputed the presence of surface plasma during laser oxygen cutting of a mild steel workpiece. They argued that the iron oxide (FeO) formed during oxygen-assisted laser cutting of mild steel does not boil because FeO does not have a gas phase but will instead dissociate into oxygen and iron when heated to sufficiently high temperatures. The dissociation of the FeO would consume much power from the cutting process and could cause a breakdown in the cutting process.

The two major cutting flaws in laser cutting of thick-section low-alloyed steel with oxygen assist gas include the cut edge surface roughness (i.e. the striation) and the dross formation on the lower cut edge. The challenge in obtaining a high cut quality in oxygen-assisted laser cutting especially in the case of thick-section steel comes from the extent of the exothermic reaction which influences the erosion of the cut edge and development of striations on the cut edge. Yilbas [**8**] examined the oxygen-assisted laser cutting of 12 mm thick mild steel sheet using a CO_2 laser and reported that the laser power intensity and oxygen pressure had significant effects on kerf width variation. Tani *et al.* [**9**] reported that the two mechanisms responsible for dross adhesion include the surface tension of the melt, which limits the melt-ejection speed, and the build-up of melt at the bottom of the kerf, which results in incomplete ejection of the molten material. Ivarson [**10**] investigated the level of thermal loss by conduction during oxygen-assisted laser cutting of mild steel and stainless steel workpieces. He reported that the power contribution by the oxidation reaction becomes larger with increase in material thickness such that there is a threshold maximum thickness for each laser power level above which the power of the oxidation reaction exceeds the laser power. The efficiency and rate of the oxidation reaction are proportional to the heated surface area of the cut zone and therefore proportional to the workpiece thickness. Additionally, single and multiple reflections take place inside the thick-section cut kerfs resulting in increased absorption of the incident laser beam towards the bottom of the cut. The power loss from the cut front by conduction also increases, in an approximately linear manner, with increase in material thickness.

The current paper examines the laser power requirement for oxygen-assisted laser cutting of 15 mm mild steel and nitrogen-assisted laser cutting of 10 mm stainless steel workpieces using a high-power fibre laser and a CO_2 laser. The laser power requirement for melting the kerf volume plus the inevitable conduction power losses at a given cutting speed is calculated using the lumped-parameter formulation method. The calculated laser power requirement at a given cutting speed is compared with the incident laser power used in cutting tests of the 15 mm mild steel with oxygen assist gas and 10 mm stainless steel with nitrogen assist gas using a multi-mode 5 kW fibre laser and a 4 kW CO_2 laser. The effects of process parameters on the cut kerf quality in mild steel laser cutting with oxygen assist

gas are analysed, whereby the cut quality obtained in 15 mm mild steel cutting with the high-power fibre laser is presented.

2 THEORETICAL ANALYSIS OF POWER REQUIREMENT

The power balance contributions in oxygen-assisted laser cutting of mild steel include the absorbed laser power and reaction power from the exothermic oxidation reaction as the incoming power terms, while stainless steel laser cutting using nitrogen assist gas employs only the absorbed laser power as the incoming power contribution. In both cases the power used for melting the kerf volume and the inevitable conduction power losses from the cutting zone to the substrate metal constitute the outgoing power terms. The melt film is generated by the melting action of the absorbed laser power and the oxidation reaction power, and is sheared by the action of the assist gas jet. The rate of melting (corresponding to the cutting speed) that can be achieved under given cutting conditions must correspond to the rate of melt removal from the cut kerf so as to maintain a high-quality cutting process and high cut quality. The melting efficiency during the cutting process is determined by the amount of laser power absorbed in the cutting zone and utilized in the melting of the kerf volume.

2.1 Laser cutting of mild steel with oxygen

The power balance for a steady-state laser oxygen cutting of a steel substrate depicted in Fig. 1 can be expressed using a lumped-parameter formulation presented in equation (1); the incoming power to the cutting zone (the absorbed laser power and the reaction power) must be equal to the outgoing power from the cutting zone, i.e. the heat content of the melted kerf volume including the latent heats for phase change and the conductive power loss to kerf sides [**11**]. The power losses by radiation to air in top and root side are typically considered to be negligible. It is assumed that all the melted material is removed to form the cut kerf and the kerf sides are heated but not melted, so that the width of the melting front is equivalent to the kerf width

$$AP_{\mathrm{L}} + P_{\mathrm{R}} = \rho w d V \left(C_{\mathrm{P}} \Delta T + L_{\mathrm{m}} + \beta L_{\mathrm{V}}\right) + P_{\mathrm{Loss}} \qquad (1)$$

In equation (1), A is the absorptivity of the workpiece to the laser radiation, P_{L} the incident laser power, P_{R} the reaction power, ρ the workpiece material density, w the kerf width, d the workpiece thickness, V the cutting speed, C_{P} the specific heat of the workpiece material, ΔT the temperature change of the melted kerf volume, L_{m} the latent heat of melting, β the fraction of the kerf volume that is vaporized, L_{V} the latent heat of vaporization, and P_{Loss} the conductive power loss to the kerf sides.

For a steady cutting process, it is assumed that the whole molten material will be removed in the molten state and the fraction of the kerf volume that is vaporized is $\beta = 0$ [**8**], so that equation (1) reduces to

$$AP_{\mathrm{L}} + P_{\mathrm{R}} = \rho w d V \left(C_{\mathrm{P}} \Delta T + L_{\mathrm{m}}\right) + P_{\mathrm{Loss}} \qquad (2)$$

The laser power absorbed by the workpiece AP_{L} will be higher when the absorptivity A of the workpiece to the incident laser radiation is higher, so that the incident laser beam power P_{L} required for cutting at a particular cutting speed will be lower. The power loss from the cutting zone during laser cutting of metals is mainly due to thermal conduction from the cutting zone to the bulk material through the kerf sides. The heat conduction in the x-direction (cutting direction) in Fig. 1 is regarded as power utilized for cutting and the liquid–solid interface is at the melting temperature throughout the cut depth, so that the power loss from the cutting zone to the substrate metal can be considered to be due only to the temperature gradient in the y-direction (kerf sides). The heat efflux from the cutting zone to the substrate metal by thermal conduction through the kerf sides can then be estimated using equation (3) by considering the temperature gradient on the kerf sides and the surface area of the cut edge [**12**]

$$P_{\mathrm{Loss}} = 2 \oint -k \nabla T \, \mathrm{d}A \qquad (3)$$

where k is the thermal conductivity, T the workpiece temperature, and dA is the surface area of the cut edge.

Schulz *et al.* [**13**] developed an analytical approximation of the heat conduction losses during laser cutting of metals. By using their expression for the temperature change ΔT_{Loss} in the substrate metal given in equation (4a), one can estimate the power loss to the bulk material using equation (5) when a

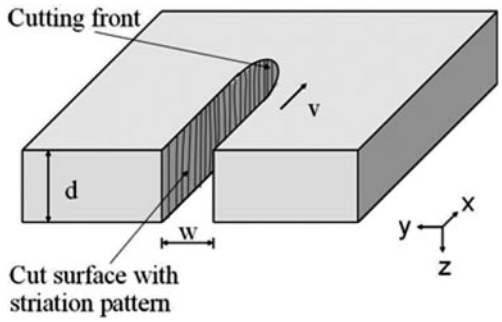

Fig. 1 Schematic illustration of the laser-cut kerf

cut slot is made in a workpiece of thickness d at a cutting speed V and the cut slots are made at a distance L from each other. The boundary separating the molten kerf volume and the solid kerf sides is at the melting isotherm, so that the kerf sides are taken to be at the melting temperature T_m and the edges of the workpiece to be at the ambient temperature T_{amb} (room temperature 298 K)

$$\Delta T_{Loss} = \frac{r_0(T_m - T_{amb})}{L}\left(\frac{Pe}{2}\right)^{-0.7} \quad (4a)$$

$$Pe = \frac{r_0 V}{\alpha} \quad (4b)$$

$$P_{Loss} = 2\int \rho C_P \Delta T_{Loss}\, dx dy dz = 2\left(\rho C_p \Delta T_{Loss} VLd\right) \quad (5)$$

where r_0 is the distance from the beam centre to the kerf sides, T the workpiece temperature, Pe the Peclet number, and α the thermal diffusivity.

The exothermic oxidation reaction that takes place during oxygen-assisted laser cutting of a steel workpiece is facilitated by diffusion and mass transfer of the oxygen and iron ions in the molten layer. The extent of the oxidation reaction ($Fe + {}^1/_2O_2 \rightarrow FeO$) is determined by the amount of metal or oxygen consumed in the reaction or the amount of oxide produced [**14**]. Therefore the exothermic oxidation reaction power P_R can be estimated from the power P_{O_2} made available by the oxygen flow to the cutting front or from the power P_{Fe} made available by the molten material flow into the interaction zone [**15**]. Only a small proportion of the oxygen jet is consumed in the reaction; part of it is lost across the top surface of the sheet or down the back side of the kerf and the rest is used as thrust to blow the melt out of the cut kerf. Ivarson [**10**] analysed the particles ejected during laser cutting of mild and stainless steel and reported that approximately half the iron which leaves the cut zone is oxidized to iron oxide (FeO). The powers P_{O_2} and P_{Fe} can then be estimated using equations (6a) and (6b) and the minimum value of these two powers will be the maximum reaction power added to the cutting process by the oxidation reaction, because the reaction is limited by the flow rate of the rarer type of reactant (either oxygen or iron)

$$P_{O_2} = (\pi/4) w^2 v_{O_2} \rho_{O_2} E_{OX}/m_{O_2} \quad (6a)$$

$$P_{Fe} = \frac{1}{2}(wd\, V \rho\, E_{OX}/m_{Fe}) \quad (6b)$$

In equations (6a) and (6b), v_{O_2} is the oxygen velocity (depending on the gas pressure), ρ_{O_2} the oxygen density, E_{OX} the energy per single reaction, m_{O_2} the molar mass of oxygen, and m_{Fe} the molar mass of iron.

2.2 Oxidation reaction kinetics

The oxygen pressure influences the exothermic oxidation reaction through the concentration of oxygen gas at the cutting zone. According to Fick's law described by equation (7), the rate of mass transfer N of the diffusing reactants (Fe^{2+} or O^{2-}) is proportional to the local concentration gradient of the diffusing reactant dC/dr, where the proportionality constant D is the diffusion coefficient. When the molten iron is exposed to the oxygen jet, an exothermic oxidation reaction is ignited and the amount of oxygen dissolved in the molten iron, and consequently the oxidation rate, increases with the square root of the oxygen pressure. In order for the oxidation reaction to proceed further at the reaction front shown schematically in Fig. 2, the Fe^{2+} ions must be transported through the oxide (FeO) film towards the oxide–gas interface and the O^{2-} ions must be transported across the oxide film towards the oxide–melt interface. In high-temperature oxidation of iron, the diffusion of the Fe^{2+} ions across the oxide layer is the rate-controlling process so that the FeO grows at the oxide–gas interface [**14**, **16**–**18**]

$$N = -D\frac{dC}{dr} \quad (7)$$

The diffusion length L_D of the reactant ions (Fe^{2+} or O^{2-}) in a given direction in time t is given by equation (8). The diffusion length, which increases as the square root of the diffusion time t, is the measure of how far the mass transfer of the reactant ions has propagated by diffusion in a given time [**16**, **18**]

$$L_D = \sqrt{2Dt} \quad (8)$$

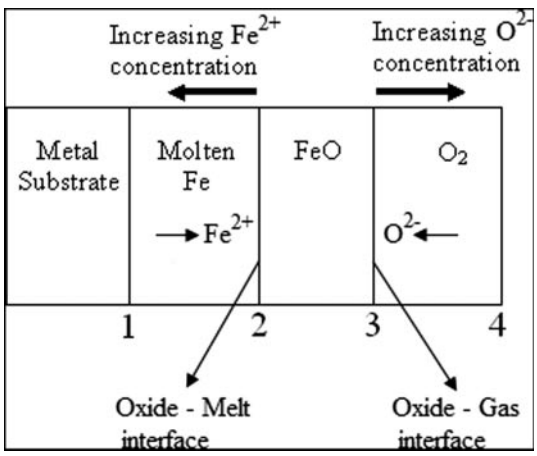

Fig. 2 Schematic illustration of the reaction front

Table 1 Thermophysical properties [**8, 16, 19, 20**]

Property	Units	Mild steel	Stainless steel	Oxygen
Density, ρ	kg/m^3	7850	8030	1.308
Specific heat capacity, C_P	J/kg·K	490	500	–
Thermal diffusivity, α	m^2/s	12×10^{-6}	4×10^{-6}	–
Latent heat of melting, L_m	J/kg	270×10^3	300×10^3	–
Melting temperature, T_m	K	1808	1712	–
Ambient temperature, T_{amb}	K	298	298	–
Energy per reaction, E_{OX}	J/mol	250×10^3	–	250×10^3
Molar mass, m_{Fe} and mo_2	kg/mol	55.8×10^{-3}	–	32×10^{-3}

Table 2 Workpiece and process parameters

Parameter	Unit	Value
Cutting speed, V	m/min	0.2–2.0
Workpiece thickness, d	m	0.015 (mild steel) 0.010 (stainless steel)
Kerf width, w	m	0.001
Distance between cut slots, L	m	0.02
Distance from beam centre to kerf sides, r_0	m	0.0005
Oxygen pressure	bar	1.0

Table 3 Laser parameters

Parameter	Units	Fibre laser	CO_2 laser
Max. laser power	kW	5	4
Nominal beam quality (BPP)	mm·mrad	5.2	6.5
Beam delivery fibre	μm	150	not applicable
Focal length	mm	190.5	190.5
Min. focused spot diameter	mm	0.3	0.3

2.3 Laser cutting of stainless steel with nitrogen

Stainless steel laser cutting using nitrogen assist gas employs only the absorbed laser power as the incoming power contribution. For a pure fusion cutting process where the kerf volume must only be melted but not vaporized (i.e. the fraction of the kerf volume that is vaporized is $\beta = 0$), equation (1) reduces to

$$AP_L = \rho w d V \left(C_P \Delta T + L_m\right) + P_{Loss} \tag{9}$$

Table 1 gives the values of the thermophysical properties of the mild steel, stainless steel, and oxygen and Table 2 gives the gas pressure and workpiece and kerf dimensions. These values were used for calculation of the laser power required for cutting a mild steel workpiece with oxygen assist gas and a stainless steel workpiece with nitrogen assist gas using equations (2), (4) to (6), and (9).

3 EXPERIMENTAL INVESTIGATION

Cutting experiments were undertaken using an IPG YLR-5000 fibre laser with maximum power output of 5 kW and a Trumpf TruLaser 3530 with maximum output power of 4 kW. The laser system parameters are given in Table 3. The test materials were 15 mm mild steel (Laser 355MC) plate and 10 mm stainless steel (1.4301) plate with typical chemical compositions given in Table 4. The assist gas delivered through a conical nozzle tip was oxygen for mild steel cutting and nitrogen for stainless steel cutting. The workpieces were prepared into sizes of 200 mm $\times$ 150 mm and cut slots of 100 mm length were made at a distance of 20 mm apart. The process parameters examined included laser power, cutting speed, assist gas pressure, and nozzle diameter; the cutting process variables used are given in Table 5. The focal position was defined as positive (+) for focus above the top surface of the workpiece and negative (–) for focus below the top surface of the workpiece. Physical observations of the cut edges were made to investigate the conditions which influenced dross attachment and kerf width variation. A microscope equipped with a camera was used to capture images of the cut kerfs from which the average kerf width was measured using the UTHSCSA ImageTool program. Scanning electron microscopy was used to obtain micrographs of the laser-cut cross-sections in order to investigate the effects of process parameters on the striation pattern; and X-ray dispersion analysis was made to determine the chemical composition of the dross as a means of examining the level of oxidation of the melt.

4 RESULTS AND DISCUSSION

The calculated laser power required for cutting a 15 mm mild steel workpiece using oxygen assist gas and a 10 mm stainless steel workpiece using nitrogen assist gas is presented and compared with the incident laser power in the cutting tests using the high-power fibre laser and the CO_2 laser. The cutting quality obtained in laser oxygen cutting of the 15 mm mild steel workpiece using the fibre laser and the

Table 4 Typical chemical compositions of workpiece materials [**21, 22**]

Mild steel (Laser 355MC)							
Element	C	Si	Mn	P	S	Al	Fe
Content (wt%)	0.12	0.03	1.50	0.020	0.015	0.015	balance
Stainless steel (1.4301)							
Element	C	Cr	Ni	Fe			
Content (wt%)	Max. 0.07	18.1	8.2	balance			

Table 5 Process variables

Parameter (units)	Levels	Increment
Laser power (kW)	1–5	1
Cutting speed (m/min)	0.2–2.0	0.2
O_2 pressure (bar)	0.2–1.2	0.2
N_2 pressure (bar)	18	–
Nozzle diameter (mm)	1.5–2.5	0.5
Focal length (mm)	190.5	–
Focal position (mm)		
Mild steel	–10, –12	–
Stainless steel	–8	–

effects of the cutting parameters on the cutting quality, including kerf width variation, dross attachment, and striation pattern, are presented.

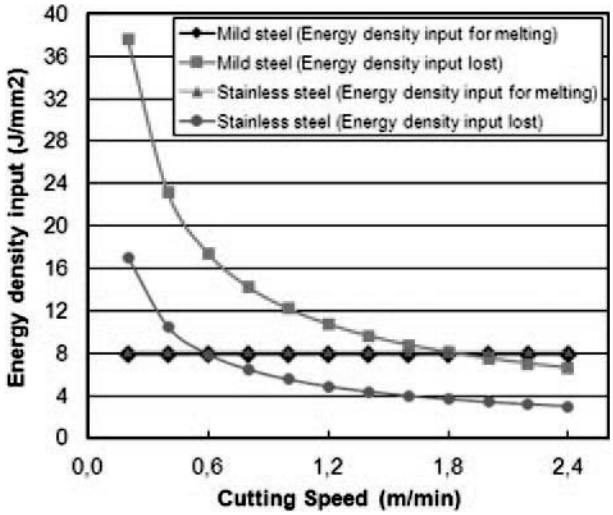

Fig. 3 Calculated energy density input for melting and energy density input lost

4.1 Laser power requirement

The total energy required for melting the kerf volume increases with cutting speed due to an increase in the rate of melting, but the energy for melting a unit area is constant (see Fig. 3). At lower cutting speeds the conduction energy loss per unit area is higher than the energy used for melting a unit area. The conduction energy loss per unit area decreases drastically with increase in cutting speed and a certain high cutting speed is reached beyond which the energy loss per unit area is lower than the energy for melting a unit area. This means that the cut workpiece is heated to higher temperatures during a slower cutting process than when a higher cutting speed is applied. The lower conduction energy loss at higher cutting speed is a consequence of the steeper temperature gradients with increase in cutting speed, and the heating effect is concentrated to the cutting zone with less heat spreading to the substrate metal. Therefore the efficiency of the cutting process increases with increase in cutting speed because a higher proportion of the absorbed laser power will be used for melting the kerf volume than is lost to the substrate metal through heat conduction from the cutting zone.

The maximum achievable cutting speed for a given laser power is defined as the maximum cutting speed at which the cut edges are separated. It is apparent that the maximum cutting speed for a given laser power is also highly influenced by the efficiency of the melt removal from the cut kerf. The mild steel cut edges produced at the highest cutting speeds may be rejoined at the bottom of the cut kerf by re-solidified melt as a result of poor melt removal at the bottom of the cut kerf. Figures 4 and 5 show comparisons of the calculated laser power requirement (melting power and inevitable conduction power losses) with the experimental incident laser power for the cutting of a 15 mm mild steel workpiece and 10 mm stainless steel workpiece using the high-power fibre laser and CO_2 laser. For both mild steel cutting and stainless steel cutting, the incident laser power required for cutting at a given cutting speed was lower when cutting was performed with the fibre laser than when the CO_2 laser was used. This indicates a higher absorption of the fibre laser beam by the workpiece, giving a higher melting efficiency than that of the CO_2 laser beam. The proportion of the incident laser beam power that is absorbed (absorptivity A) during laser cutting of the stainless steel workpiece can be estimated from Fig. 5 using equation (10). The estimated absorptivity during stainless steel cutting was greater than 60 per cent with the fibre laser and less than 60 per cent with the CO_2 laser. The total laser power absorbed by the workpiece increases after the cutting front is formed and a constant melting front is maintained because of the temperature dependence of absorptivity resulting in increased laser beam absorption at the melt surface. Also increased laser beam absorption in the cut kerf is realized through

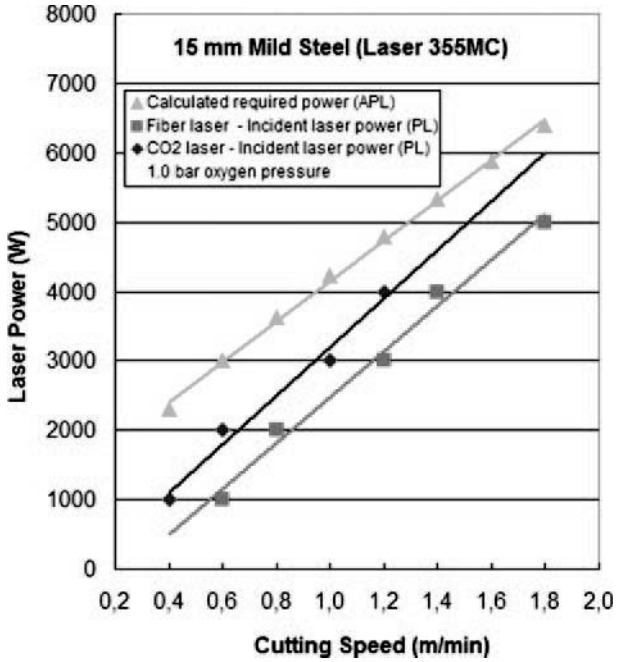

Fig. 4 Power required for laser cutting 15 mm mild steel

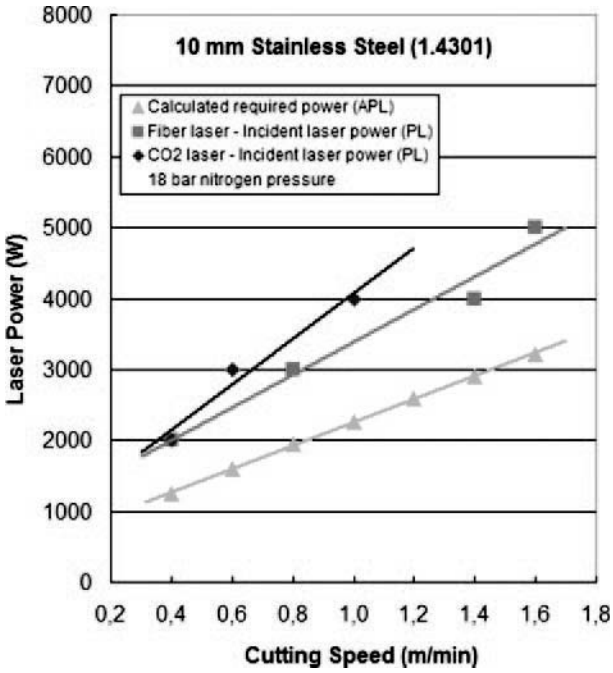

Fig. 5 Power required for laser cutting 10 mm stainless steel

the multiple reflections of the laser beam in the thick-section cut kerf

$$\text{Absorptivity}(A) = \frac{\text{Required laser power}\,(AP_{\text{L}})}{\text{Incident laser power}\,(P_{\text{L}})} \tag{10}$$

In the case of mild steel laser cutting with oxygen assist gas, the incident laser power at a given cutting speed for both the fibre laser and CO_2 laser was lower than the calculated required laser power for melting the kerf volume and compensation of inevitable conduction losses (see Fig. 4). The reason for this scenario is that a higher reaction power was realized in the cutting tests than was estimated in the calculations because the oxidation reaction is influenced by process parameters such as cutting speed, oxygen pressure, and nozzle diameter.

4.2 Effect of process parameters in mild steel laser oxygen cutting

Thick-section mild steel laser cutting using oxygen assist gas produces a larger amount of melt and employs lower cutting speeds than in thin-section cutting; therefore the influences of the oxidation reaction on the cutting quality are more severe than in thin-section cutting.

4.2.1 Effect of cutting speed

The kerf width variation with deep grooves on the cut surface in laser oxygen cutting of mild steel is caused by the erratic sideways burning oxidation reaction favoured by lower cutting speed (Fig. 6(a)). High-speed cutting can produce a more uniform cut kerf with a periodic pattern of ridges along the cut length, which is typical of the widely accepted mechanism for striation formation based on the cyclic sideways burning effects during laser oxygen cutting of mild steel as originally explained by Arata *et al.* [**23**] and Miyamoto and Maruo [**24**]. However, the higher rate of melting at high cutting speeds results in melt build-up at the lower section of the cut kerf, causing dross attachment on the lower cut edges, and in worst cases the cut edges are rejoined at the bottom section by the re-solidified melt behind the keyhole (see Fig. 6(b)). The narrow cut kerfs produced at high cutting speeds increase the tendency for re-solidified melt in the cut kerf (Fig. 7). Additionally, a more viscous melt layer is produced when the level of the melt oxidation is low, resulting in a high tendency of melt re-solidification in the cut kerf. The cutting process can break down if the cutting speed is too high due to failure of the molten material in the narrow cut kerf to clear the lower cut edge at a sufficiently fast rate corresponding to the cutting speed. In such situations one can say that cutting at the given high cutting speed is limited by the melt removal rather than the power requirement. The steeper temperature gradients when cutting is performed with high cutting speed cause the oxidation reaction to be localized at the cutting front without spreading sideways to widen the cut kerf. During a slow cutting process, there is much heat spread from the cutting zone and

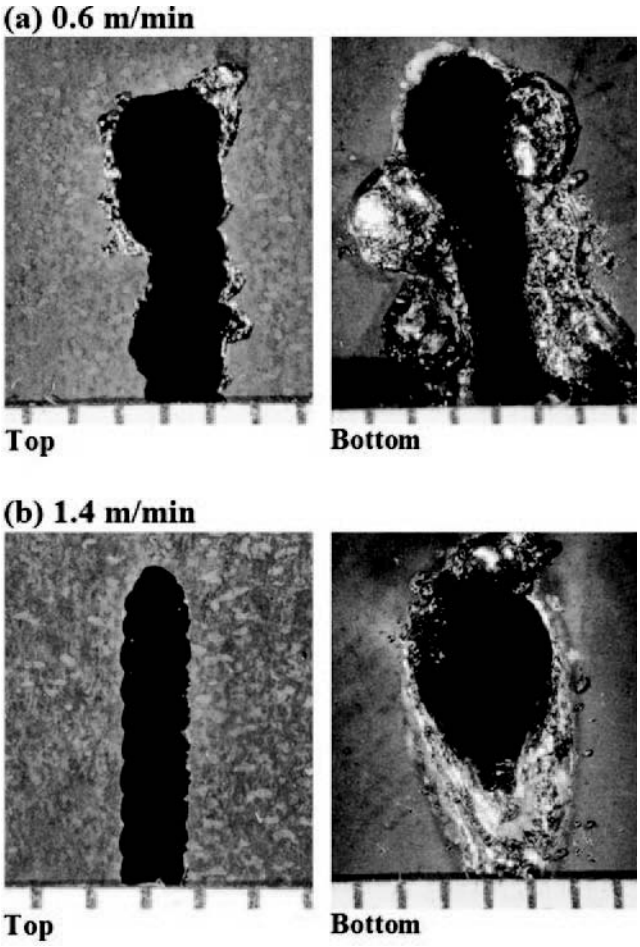

Fig. 6 Kerf width variation and dross attachment with cutting speed (15 mm mild steel, 3 kW, 1.0 bar, 2.0 mm nozzle, and –10 mm focal position)

a larger diffusion length of the reactant ions (according to equation (8)), so that the oxidation reaction spreads out from the cutting front and a higher proportion of the melt can be oxidized, thereby generating much reaction power and widening the cut kerf. The excess reaction power also causes higher conduction losses to the substrate metal followed by heat build-up in the cut workpiece.

The cutting front is inclined at high cutting speed as can be seen from the inclination of the striations with increase in cutting speed in Fig. 8. The cut edge shows two distinct striation patterns on the top section and lower section of the cut edge. The striations at the top-third section of the cut surface (primary striations) are mainly caused by the burning oxidation reaction. Melt flow integration takes place in the middle-third section of the cut surface, forming wider striations which continue to the bottom cut edge (secondary striations). The secondary striations, which are deeper and more widely spaced than the primary striations, seem to be mainly influenced by

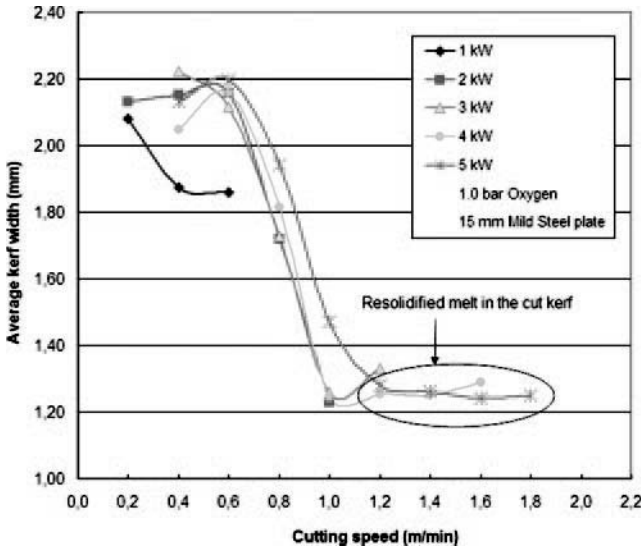

Fig. 7 Kerf width with cutting speed

the two mechanisms that cause increased erosion of the kerf sides at the lower cut section, namely:

(a) increased absorption of the laser beam at the lower cut section due to multiple reflections of the incident laser beam in the cut kerf;
(b) longer residence times of the melt at the lower cut section due to melt build-up.

These two melting effects result in deterioration of the cut edge perpendicularity and the top cut section is raised over the lower cut section.

4.2.2 Effect of oxygen pressure

The erratic nature of the oxidation reaction is minimized when cutting is performed with oxygen pressures below 1.0 bar and more uniform kerfs can be obtained (Fig. 9). The high melting efficiency of the fibre laser means that a large amount of melt is generated and the process requires that the melt is highly oxidized, so that it has a lower viscosity for effective melt removal. The rate of the oxidation reaction is favoured by high oxygen pressure (see Fig. 9(b)) because of the high concentration of the oxygen gas at the cutting zone, such that a larger melt surface is in contact with the oxygen which increases the proportion of the melt that is oxidized and a higher reaction power is generated. The excess reaction power causes excessive melting and widening of the cut kerf.

4.2.3 Effect of nozzle diameter

The best cut quality, with a fine uniform striation pattern on the cut edge, is obtained with a 1.5 mm nozzle and a 2.5 mm nozzle produces the worst cut quality. A smaller nozzle delivers a precise amount of oxygen to the interaction zone and the burning oxi-

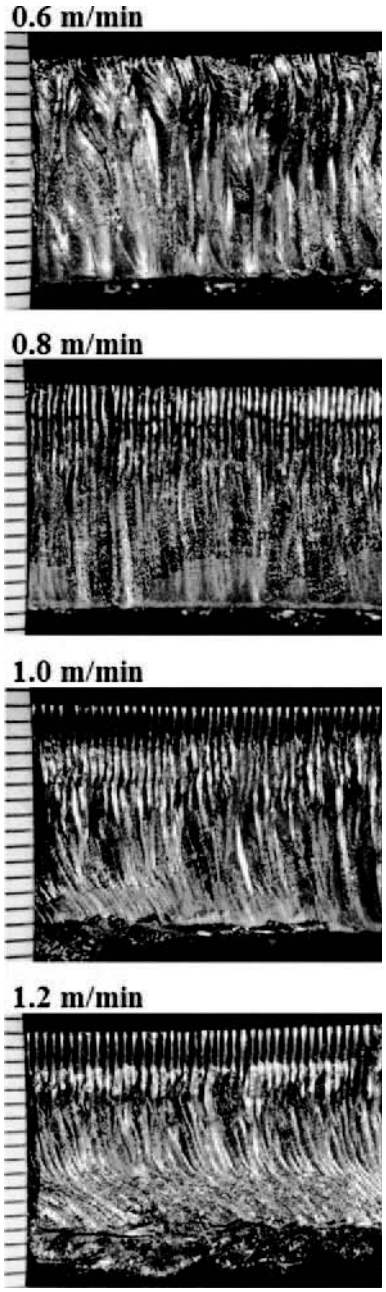

Fig. 8 Effect of cutting speed on striation inclination (15 mm mild steel, 3 kW, 1.0 bar, 2.0 mm nozzle, and –10 mm focal position)

dation reaction is localized to the cutting front, producing more uniform cut kerfs with finer, closely spaced striations on the cut edge. On the other hand, a larger nozzle delivers an increased amount of oxygen gas into the cutting zone resulting in an erratic burning oxidation reaction, and a wider non-uniform cut kerf is produced with deeper widely spaced striations. The melt surface is highly oxidized while the underlying melt is only partially oxidized or not oxidized at all; the level of oxidation of the melt surface also varies from point to point as shown by the chemical composition of the dross in Fig. 10. The

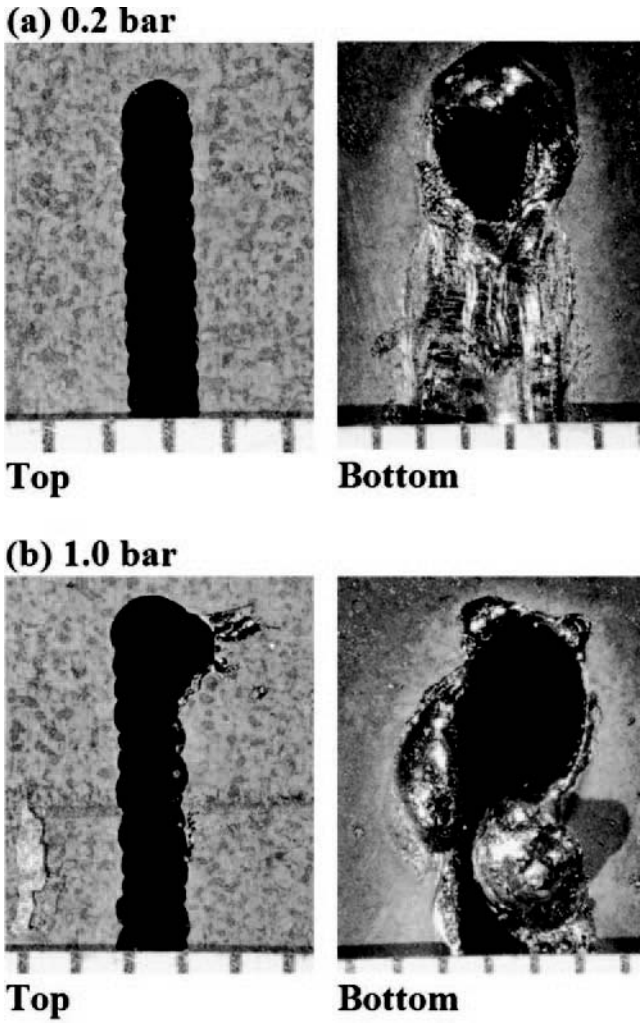

Fig. 9 Kerf width variation and dross attachment with oxygen pressure (15 mm mild steel, 3 kW, 0.8 m/min, 2.0 mm nozzle, and –10 mm focal position)

melt shearing effect of the oxygen jet means that new melt can be exposed periodically for continuous oxidation of the melt layer and clean cut edges can be obtained under optimum cutting conditions, like when a smaller nozzle diameter is used (see Fig. 10 (a)). Otherwise, the increased amount of melt produced when a larger nozzle is used results in inefficient removal of the highly viscous, unoxidized underlying melt layer and the re-solidified melt remains firmly attached to the lower cut edges (see Fig. 10(b) and (c)).

5 CONCLUSIONS

Laser power requirement for the cutting of thick-section mild steel and stainless steel using the high-power fibre laser and CO_2 laser was investigated in this study. The calculated laser power requirement for melting the kerf volume plus the inevitable

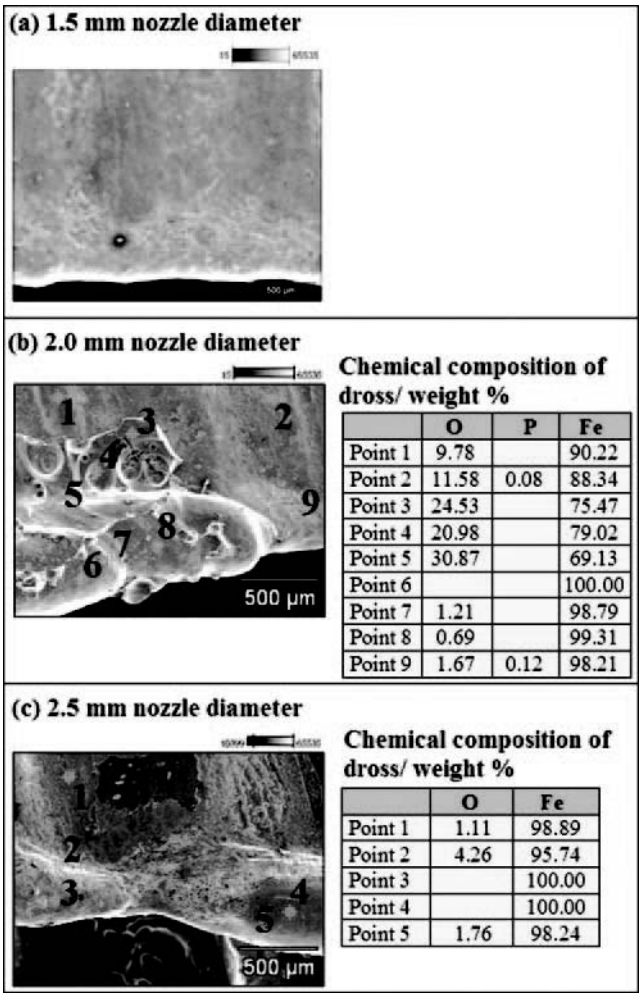

	O	P	Fe
Point 1	9.78		90.22
Point 2	11.58	0.08	88.34
Point 3	24.53		75.47
Point 4	20.98		79.02
Point 5	30.87		69.13
Point 6			100.00
Point 7	1.21		98.79
Point 8	0.69		99.31
Point 9	1.67	0.12	98.21

	O	Fe
Point 1	1.11	98.89
Point 2	4.26	95.74
Point 3		100.00
Point 4		100.00
Point 5	1.76	98.24

Fig. 10 Chemical composition of dross (15 mm mild steel, 3 kW, 1.0 m/min, 1.2 bar, and –12 mm focal position)

conduction power losses at a given cutting speed was compared with the incident laser power used in cutting tests of 15 mm mild steel with oxygen assist gas and 10 mm stainless steel with nitrogen assist gas using the high-power fibre laser and the CO_2 laser. For the cutting of both mild steel and stainless steel, the required incident laser power for cutting at a given cutting speed using the high-power fibre laser was found to be lower than that for the CO_2 laser, showing a higher absorption of the fibre laser beam by the workpiece. The inefficient melt removal during high-speed fibre laser cutting of the 15 mm mild steel workpiece with oxygen assist gas is attributed to the higher melting efficiency of the high-power fibre laser, where the absorptivity was estimated to be greater than 60 per cent.

The partially oxidized melt at the maximum cutting speeds had a high viscosity, resulting in dross formation and in the worst cases re-solidified melt in the cut kerf due to poor melt removal at the bottom section of the cut kerf. The process parameters that influence the amount of reaction power addition to the cutting process, namely gas pressure, nozzle diameter, and cutting speed, were found to play a critical role in obtaining a high cutting quality because these parameters influence the rate of melting as well as the rate of melt removal from the cut kerf. Optimization of these process parameters is critical for controlling the sideways burning exothermic oxidation reaction and achievement of efficient melt removal. The size of the striations decreased with increase in cutting speed, decrease in oxygen pressure, and reduction in nozzle diameter, and the cut quality improved under these cutting conditions.

ACKNOWLEDGEMENT

The authors wish to express their gratitude to the company HT Laser Oy for funding this research, Mr Pasi Pänkäläinen for performing the CO_2 laser cutting tests, and Mr Pertti Kokko for performing the fibre laser cutting tests.

REFERENCES

1 **Wandera, C., Salminen, A., Olsen, F. O.,** and **Kujanpää, V.** Cutting of stainless steel with a fiber and disk laser. In Proceedings of the 25th International Conference on *Lasers and electro optics (ICALEO)* Scottsdale, Arizona, USA, 30 October–2 November 2006, pp. 211–220 (Laser Institute of America, Orlando, Florida, USA).

2 **Sparkes, M., Gross, M., Celotto, S., Zhang, T.,** and **O'Neill, W.** Inert cutting of medium section stainless steel using a 2.2 kW high power fibre laser. In Proceedings of the 25th International Conference on *Lasers and electro optics (ICALEO)* Scottsdale, Arizona, USA, 30 October–2 November 2006, pp. 197–205 (Laser Institute of America, Orlando, Florida, USA).

3 **Xie, J., Kar, A., Rothenflue, J. A.,** and **Latham, W. P.** Temperature-dependent absorptivity and cutting capability of CO_2, Nd:YAG and chemical oxygen–iodine lasers. *J. Laser Applic.*, 1997, **9**, 77–85.

4 **Mahrle, A., Bartels, F.,** and **Beyer, E.** Theoretical aspects of the process efficiency in laser beam cutting with fiber lasers. In Proceedings of the 27th International Conference on *Applications of lasers and electro optics (ICALEO)* Temecula, California, USA, 22–23 October 2008, pp. 703–712 (Laser Institute of America, Orlando, Florida, USA).

5 **Golnabi, H.** and **Bahar, M.** Investigation of optimum condition in oxygen gas-assisted laser cutting. *Optic. Laser Technol.*, 2009, **41**, 454–460.

6 **Yilbas, B. S.** Experimental investigation into CO_2 laser cutting parameters. *J. Mater. Process. Technol.*, 1996, **58**, 323–330.

7 **Powell, J., Petring, D., Kumar, R. V., Al-Mashikhi, S. O., Kaplan, A. F. H.,** and **Voisey, K. T.** Laser–oxygen cutting

of mild steel: the thermodynamics of the oxidation reaction. *J. Phys. D: Appl. Phys.*, 2009, **42**, 1–11.
8 **Yilbas, B. S.** Laser cutting of thick sheet metals: effects of cutting parameters on kerf size variations. *J. Mater. Process. Technol.*, 2008, **201**, 285–290.
9 **Tani, G., Tomesani, L.,** and **Campana, G.** Prediction of melt geometry in laser cutting. *Appl. Surf. Sci.*, 2003, **208–209**, 142–147.
10 **Ivarson, A.** *On the physics and chemical thermodynamics of laser cutting*, Doctoral Thesis (1993:114, papers I and II), Department of Applied Physics and Mechanical Engineering, Luleå University of Technology, 1993.
11 **Welty, J. R..** *Engineering heat transfer SI version*, 1978, pp. 20–25 (John Wiley & Sons, Chichester, UK).
12 **Carslaw, H. S.** and **Jaeger, J. C.** *Conduction of heat in solids*, edition 2, 1959, pp. 6–9 (Clarendon Press, Oxford, UK).
13 **Schulz, W., Becker, D., Franke, J., Kemmerling, R.,** and **Herziger, G.** Heat conduction losses in laser cutting of metals. *J. Phys. D: Appl. Phys.*, 1993, **26**, 1357–1363.
14 **Birks, N.** and **Meier, G. H.** *Introduction to high temperature oxidation of metals*, 1983, pp. 2, 31–43 (Edward Arnold Ltd, London).
15 **Ready, J. F.** and **Farson, D. F.** (Eds) *LIA handbook of laser materials processing,* 2001, pp. 428–430 Laser Institute of America, Orlando, Florida, USA.
16 **Callister, W. D.** *Materials science and engineering: An introduction*, edition 6, 2003, pp. 95–99, 758 (John Wiley & Sons, Chichester, UK).
17 **Kay, J. M.** and **Nedderman, R. M.** *An introduction to fluid mechanics and heat transfer*, edition 3, 1974, p. 11 (Cambridge University Press, Cambridge, UK).
18 **Kubaschewski, O.** and **Hopkins, B. E.** *Oxidation of metals and alloys*, 1953, pp. 1–4, 20–26, 46–54 (Butterworth Scientific Publications Ltd, London).
19 **Bäuerle, D.** *Laser processing and chemistry*, edition 3, 2000, pp. 695, 705 (Springer-Verlag, Berlin/Heidelberg, Germany).
20 **Lide, D. R.** (Ed.) *CRC handbook of chemistry and physics* edition 89, 2008–2009, section 4, pp. 68, 79; available from http://www.hbcpnetbase.com/ (access date 5 October 2009).
21 **Anon.,** Hot Rolled Plates, Sheets and Coils; available from http://www.ruukki.com/www/materials.nsf/materials/320D13CB0912BDD7C225723600408B24/$File/Laser_04.2006_EN.pdf?openElement (access date 1 October 2009).
22 **Anon.,** EN 1.4301, AISI 304; EN 1.4307, AISI 304L, Outo Kumpu product information, 2009; available from http://www.outokumpu.com/43395.epibrw (access date 1 October 2009).
23 **Arata, Y., Maruo, H., Miyamoto, I.,** and **Takeuchi, S.** Dynamic behavior in laser gas cutting of mild steel. *Trans. JWRI*, 1979, **8**, 15–26.
24 **Miyamoto, I.** and **Maruo, H.** The mechanism of laser cutting. *Welding in the World (UK)*, 1991, **29**, 283–294.

APPENDIX 1

Notation

A	absorptivity
C_P	specific heat capacity
d	workpiece thickness
dA	surface area of the cut edge
dC/dr	concentration gradient of the diffusing reactant
D	diffusion coefficient
E_{OX}	energy per single oxidation reaction
k	thermal conductivity
L	distance between cut slots
L_D	diffusion length of the reactant ions
L_m	latent heat of melting
L_V	latent heat of vaporization
m_{Fe}	molar mass of iron
m_{O_2}	molar mass of oxygen
N	rate of mass transfer of the diffusing reactants
Pe	Peclet number
P_L	incident laser power
P_{Loss}	conduction power loss to the kerf sides
P_R	exothermic oxidation reaction power
r_0	distance from the beam centre to the kerf sides
t	diffusion time (cutting rate)
T	workpiece temperature
T_{amb}	ambient temperature (298 K)
T_m	melting temperature
v_{O_2}	velocity of oxygen jet
V	cutting speed
w	kerf width
x	cutting direction
y	direction perpendicular to cutting direction
α	thermal diffusivity
β	fraction of the kerf volume that is vaporized
ΔT	temperature change of kerf volume
ΔT_{Loss}	temperature change in the substrate metal
ρ	workpiece density
ρ_{O_2}	oxygen density